Geochemical evidence for widespread euxinia in the Later Cambrian ocean

Sulphur isotope evidence for widespread euxinia in the Later Cambrian ocean

Benjamin C. Gill[1*], Timothy W. Lyons[1], Seth A. Young[2], Lee R. Kump[3], Andrew H. Knoll[4], and Matthew R. Saltzman[5]

[1]Department of Earth Sciences, University of California, Riverside, 900 University Avenue, Riverside, CA, 92521, USA
[2]Department of Geological Sciences, Indiana University-Bloomington, 1001 East 10th Street Bloomington, IN 47405-1405, USA
[3]Department of Geosciences, Penn State University, 503 Deike Building, University Park, PA 16802, USA
[4]Department of Organismic and Evolutionary Biology, Harvard University, 26 Oxford Street, Cambridge, MA, 02138, USA.
[5]School of Earth Science, The Ohio State University, 275 Mendenhall Laboratory, 125 South Oval Mall, Columbus, Ohio 43210, USA
*Corresponding Author, present address: Department of Earth and Planetary Sciences Harvard University, 20 Oxford Street, Cambridge, MA, 02138, USA.

Global-scale anoxia in the deep ocean is frequently invoked as a primary driver of mass extinction, as well as a long-term inhibitor of evolutionary radiation on the early Earth. In recent biogeochemical studies, it has been hypothesized that oxygen deficiency was widespread in subsurface water masses of later Cambrian oceans[1,2], possibly influencing evolutionary events during this time[1,2,3]. Physical evidence of widespread anoxia in Cambrian oceans has remained elusive, and thus its potential relationship to the paleontological record remains largely unexplored. Here, we present sulphur isotope records from six globally distributed stratigraphic sections of later Cambrian marine rocks (ca. 499 million years old) that show a positive excursion in phase with the well-known Steptoean Positive Carbon Isotope Excursion (SPICE). Numerical box modeling of the paired carbon-sulphur isotope

data indicates that these isotope shifts reflect transient increases in the burial of organic carbon and pyrite sulphur in sediments deposited under ocean-scale anoxic and sulphidic (euxinic) conditions. Independently, molybdenum abundances in a coeval black shale point convincingly to ocean-scale anoxia. These results identify the SPICE interval as the best characterized ocean anoxic event in the pre-Mesozoic ocean and an extreme example of oxygen deficiency in the later Cambrian deep ocean. Thus, a redox structure similar to those in Proterozoic oceans[4,5,6] may have persisted or returned in the oceans of the early Phanerozoic Eon. Indeed, the environmental challenges presented by widespread anoxia may have been a prevalent if not dominant influence on animal evolution in Cambrian oceans.

Carbonate rocks of Cambrian age preserve large, rapid (of a few million years duration or less) and globally correlated excursions in the marine carbon isotope record ($\delta^{13}C_{carb}$), which indicate perturbations in the global carbon cycle (Figure S1)[7,8,9,10]. The mechanisms that drove these events, however, are poorly known. What makes these excursions particularly interesting to geobiologists is the observation that many coincide with biological events recorded by fossils, suggesting causal links between biological and environmental history[3,10]. The focus of our work is on the last large excursion of the period, the Steptoean Positive Carbon Isotope Excursion, or SPICE.

The SPICE is recorded as a +4-6‰ shift in $\delta^{13}C_{carb}$ that occurs globally in later Cambrian successions (at the beginning of the Furongian International Series and Paibian International Stage, 499 Ma); it is thought to have lasted on the order of 2-4 million

51 years[10,11]. A well-documented extinction of trilobites coincides with the onset of the
52 SPICE on the paleocontinent of Laurentia[10,12], and the isotopic excursion has also been
53 correlated to intervals of biological turnover on other paleocontinents[13]. The SPICE is
54 also coincident with global changes in sea level; its onset coincides with a transgressive
55 event, and its peak is concurrent with a lowstand recorded as the Sauk-II/III hiatus[10,11].
56 We report sulphur isotope data from six globally distributed stratigraphic sections
57 across the SPICE, and each reveal parallel, positive carbon and sulphur isotope
58 excursions (Figures 1, 2 and 3). These sections represent diverse sedimentary
59 environments; thus, similarities among the trends despite differences in depositional
60 conditions speak to the global and primary nature of the geochemical signals (see
61 Supplementary Materials for details of individual stratigraphic sections and data
62 supporting the preservation of the geochemical signals).
63 The SPICE sulphur isotope excursion is one of the largest identified in the
64 geologic record and is the first to be correlated globally at this scale of resolution. This
65 excursion occurs in both carbonate-associated sulphate (CAS) and pyrite, which further
66 supports a primary marine signal, and its magnitude indicates a major perturbation in the
67 global sulphur cycle. There are, however, significant differences in the details of the
68 sulphate sulphur isotope trends among basins. In particular, the pre-event $\delta^{34}S_{CAS}$
69 baseline differs among the various locations (Figure 2). While some records show
70 relatively steady sulphur isotope values before the excursion (i.e., western and eastern
71 Laurentia), the Gondwanan data show a positive trend up section before the excursion
72 (Figure 2).

Despite overarching similarities, the absolute values and amplitudes of the excursion also differ among the studied basins. The Gondwanan record is the most extreme, with $\delta^{34}S_{CAS}$ values reaching almost +70‰ and an amplitude of +35‰ (Figure 2). On the other end of the spectrum, the record in eastern Laurentia shows a peak value of +38‰ and amplitude of only +12‰ (Figure 2). These isotopic differences support the idea that the sulphur reservoir in the later Cambrian ocean was spatially heterogeneous and that sulphate concentrations were therefore low[14,15]. We also observe that the sulfate isotope excursion peaks stratigraphically slightly before the carbon isotope maximum (see Supplementary Figure S2), which suggests that the sulphate reservoir was relatively more sensitive to change than the marine pool of dissolved inorganic carbon (DIC). This state of sulphate in later Cambrian seawater differs greatly from the modern reservoir, which is relatively homogenous globally with a concentration of 28 mmol/kg (mM) and a sulphur isotope composition of +21‰. This contrast with the modern ocean indicates that the residence time of sulphate in the Cambrian ocean was much shorter.

The parallel behavior between the carbon and sulphur isotope excursions (Figures 2 and 3) suggests that the SPICE records a transient increase in the amount of carbon and sulphur buried as organic matter and pyrite (FeS_2) in marine sediments. Such parallel burial occurs in anoxic marine sediments and beneath euxinic water columns[16] — that is, beneath water columns that are both anoxic and contain free hydrogen sulphide. Organic matter fuels microbial sulphate reduction (MSR), and pyrite is formed when H_2S produced from MSR reacts with iron minerals and is buried along with the residual organic matter. Ultimately, the burial of both species results in the removal of carbon

95 and sulphur from the ocean. This coupling can result in positive isotope shifts for both
96 species in seawater: the carbon and sulphur leaving the ocean through burial are enriched
97 in ^{12}C and ^{32}S via isotope fractionations accompanying photosynthetic and MSR
98 pathways, respectively, leaving the seawater correspondingly enriched in ^{13}C and ^{34}S.
99 We tested this hypothesis by modeling the ocean inventories of carbon and
100 sulphur during the SPICE. Specifically, we constructed a simple box model that
101 simulates the cycling of each element in the ocean (see Supplementary Material for
102 details). The model shows that the isotope excursions can be replicated by transiently
103 increasing the amount of organic carbon buried by factors of 1.5 to 2.5 and pyrite sulphur
104 by factors of 2.5 to 4.5 for a duration of 0.5 to 1.5 million years (Figure 4: see
105 Supplementary Material for additional model details).
106 Importantly, our model puts quantitative constraints on the size of the marine
107 sulphate reservoir during the later Cambrian. An assumption of pre-SPICE sulphate
108 concentrations greater than 2.5 mM demands more than 8 million years for recovery of
109 $\delta^{34}S_{sulphate}$ (i.e., return to the pre-event baseline) following the SPICE (Figure S13), which
110 is unreasonable in light of the available constraints on the duration of the SPICE[11]. Our
111 simulations suggest, therefore, that the concentration of seawater sulphate was very low
112 — at or below the low end of the 2-12 mM range suggested by previous work[14,15].
113 Another important result from the model is that the predicted ratio of carbon-to-
114 sulphur (C/S) linked to this transient burial was very low: 1 to 4 moles C/mole S or 0.4-
115 1.5 g C/g S (Figure 4). In younger sediments, similar C/S ratios are only observed in
116 sediments deposited under euxinic conditions[16]. The scale of this Cambrian euxinia is

117 suggested by comparison to the Black Sea, the largest modern euxinic basin. Our
118 estimates for the transient burial flux of sulfur that caused the isotope excursion are equal
119 to 50-75 times that of the euxinic portion Black Sea[17], thus providing the first quantitative
120 evidence for global-scale euxinia in the Paleozoic ocean.

121 Our argument for increased euxinia becomes stronger when we consider that ΔS
122 may have decreased over the event (Figure 2). ΔS is the isotopic offset between
123 coexisting CAS and pyrite ($\Delta\delta^{34}S_{CAS\text{-}pyrite}$) that results from MSR and related microbial
124 pathways that lead to pyrite formation. For the two sections that have sufficient pyrite for
125 isotopic analysis (eastern Laurentia and Gondwana), there is a strikingly systematic
126 negative shift in ΔS parallel to the positive excursions in $\delta^{34}S_{CAS}$ and $\delta^{13}C_{carb}$ (Figure 2).
127 Importantly, a smaller ΔS, when applied to our model, requires greater pyrite burial to
128 explain the positive sulphur excursion. The further increase in pyrite burial results in an
129 even lower mean C/S ratio, strengthening the case for burial under euxinic conditions
130 (see Supplementary Figure S14 for sensitivity tests of ΔS). Our Cambrian sulphur
131 isotope data must record a decrease in seawater sulphate concentration associated with
132 voluminous euxinic pyrite burial during the SPICE under generally low levels of
133 sulphate.

134 Additional evidence for the expansion of euxinic conditions comes from the
135 coeval Alum Shale in Sweden, where a systematic decrease in molybdenum enrichment
136 coincides with the SPICE (Figure 3). Molybdenum is a transition metal, typically
137 enriched in organic-rich sediments deposited under euxinic conditions[18,19]. The
138 variability in molybdenum concentrations occurs despite iron proxy data that indicate

139 persistent euxinia over the interval of interest (Figure 3); the Alum basin appears to have
140 been locally euxinic before, during and after the SPICE. The suggestion then is that
141 another process drove the scale of enrichment. In short, the decline going into the SPICE
142 and increase coming out argue for a decrease in the global molybdenum inventory of
143 seawater as the euxinic conditions expanded and then contracted on a global scale[6,19,20]
144 — a scenario consistent with the predictions of the modeled C and S data. We envision
145 conditions during the SPICE to have been analogous to those during oceanic anoxic
146 events or OAEs of the Mesozoic, where the spread of euxinic conditions led to extensive
147 deposition of organic-rich, pyritic sediments in the deep ocean yielding concomitant
148 isotopic shifts in dissolved inorganic carbon[21] and seawater sulfate[22].

149 The geochemical and stratigraphic framework of the SPICE provides new insight
150 into the pronounced biological turnover associated with this event. Taken together with
151 evidence for sea-level rise, the geochemical data suggest that shoaling of toxic anoxic
152 deep waters onto the shelf led to the extinction of shelf fauna, a situation similar to that
153 envisioned for end-Permian extinctions[23]. Such a scenario was proposed previously to
154 explain recurrent later Cambrian trilobite extinctions[12] but in acknowledged absence of
155 independent constraints for such conditions.

156 Additional oscillations observed in the later Cambrian marine $\delta^{13}C$ record could
157 reflect environmental perturbations similar to the SPICE. We suggest that anoxic water
158 masses occurred widely in the subsurface of the later Cambrian ocean (i.e., below the
159 wind-mixed surface layer), a view that finds qualitative support in the stratigraphic
160 distribution of organic-rich, pyritic black shales, which peak in abundance in later

Cambrian successions[24]. If correct, the high rates of biological turnover[25] and repeated trilobite extinctions[12,26] documented for later Cambrian fossils find at least partial explanation in episodic expansion of oxygen-depleted waters. In larger terms, broad patterns of Cambrian animal evolution may reflect persistent oxygen deficiency in subsurface waters of Cambrian oceans, shedding new light on early evolution of the Phanerozoic biosphere in the wake of late Proterozoic oxygenation.

References

1 Hough, M. L. *et al.* A major sulphur isotope event at c. 510 Ma: a possible anoxia–extinction–volcanism connection during the Early–Middle Cambrian transition? *Terra Nova* **18**, 257-263 (2006).

2 Hurtgen, M. T., Pruss, S. B. & Knoll, A. H. Evaluating the relationship between the carbon and sulfur cycles in the later Cambrian ocean: An example from the Port au Port Group, western Newfoundland, Canada. *Earth Planet. Sci. Lett.* **281**, 288-297 (2009).

3 Zhuravlev, A. & Wood, R. Anoxia as the cause of the mid-Early Cambrian (Botomian) extinction event. *Geology* **24**, 311-314 (1996).

4 Canfield, D. E. A new model for Proterozoic ocean chemistry. *Nature* **396**, 450-453 (1998).

5 Poulton, S. W., Fralick, P. W. & Canfield, D. E. The transition to a sulphidic ocean ~1.84 billion years ago. *Nature* **431**, 173-177 (2004).

6 Scott, C. *et al.* Tracing the stepwise oxygenation of the Proterozoic ocean. *Nature* **452**, 456-459 (2008).

7 Brasier, M. D., Corfield, R. M., Derry, L. A., Rozanov, A. Y. & Zhuravlev, A. Y. Multiple $\delta^{13}C$ excursions spanning the Cambrian explosion to the Botomian crisis in Siberia *Geology* **22**, 455-458 (1994).

8 Saltzman, M. R., Runnegar, B. & Lohmann, K. C. Carbon isotope stratigraphy of Upper Cambrian (Steptoean Stage) sequences of the eastern Great Basin: Record of a global oceanographic event *Geol. Soc. Am. Bull.* **110**, 285-297 (1998).

9 Montanez, I. P., Osleger, D. A., Banner, J. L., Mack, L. E. & Musgrove, M. Evolution of the Sr and C isotope composition of Cambrian Oceans. *GSA Today* **10**, 1-7 (2000).

10 Saltzman, M. *et al.* A global carbon isotope excursion (SPICE) during the Late Cambrian: relation to trilobite extinctions, organic-matter burial and sea level. *Palaeogeogr. Palaeoclimatol. Palaeoecol.* **162**, 211-223 (2000).

[11] Saltzman, M. R. *et al.* The Late Cambrian SPICE ($\delta^{13}C$) Event and the Sauk II-SAUK III Regression: New Evidence from Laurentian Basins in Utah, Iowa and Newfoundland. *J. Sed. Res.* **74**, 366-377 (2004).

[12] Palmer, A. The Biomere Problem: Evolution of an Idea. *Journal of Paleontology* **58**, 599-611 (1984).

[13] Peng, S. *et al.* Global Standard Stratotype-section and Point of the Furongian Series and Paibian Stage Cambrian. *Lethaia* **37**, 365-379 (2004).

[14] Brennan, S. T., Lowenstein, T. K. & Horita, J. Seawater chemistry and the advent of biocalcification. *Geology* **32**, 473-476 (2004).

[15] Gill, B. C., Lyons, T. W. & Saltzman, M. R. Parallel, high-resolution carbon and sulfur isotope records of the evolving Paleozoic marine sulfur reservoir. *Palaeogeogr. Palaeoclimatol. Palaeoecol.* **256**, 156-173 (2007).

[16] Berner, R. Sedimentary pyrite formation: An update. *Geochim. Cosmochim. Acta* **48**, 605-615 (1984).

[17] Neretin, L. N., Volkov, I. I., Böttcher, M. E. & Grinenko, V. A. A sulfur budget for the Black Sea anoxic zone. *Deep-Sea Research Part I* **48**, 2569-2593 (2001).

[18] Emerson, S. & Huested, S. Ocean anoxia and the concentrations of molybdenum and vanadium in seawater. *Mar. Chem.* **34**, 177-196 (1991).

[19] Algeo, T. J. & Lyons, T. W. Mo–total organic carbon covariation in modern anoxic marine environments: Implications for analysis of paleoredox and paleohydrographic conditions. *Paleoceangraphy* **21**, 23 (2006).

[20] Algeo, T. J. Can marine anoxic events draw down the trace element inventory of seawater? *Geology* **32**, 1057-1060 (2004).

[21] Arthur, M. A., Dean, W. E. & Pratt, L. M. Geochemical and climatic effects of increased marine organic carbon burial at the Cenomanian/Turonian boundary. *Nature* **335**, 714-717 (1988).

[22] Adams, D. D., Hurtgen, M. T. & Sageman, B. B. Volcanic triggering of a biogeochemical cascade during Oceanic Anoxic Event 2. *Nat. Geosci.* **3**, 1-4 (2010).

[23] Wignall, P. B. & Twitchett, R. J. Oceanic Anoxia and the End Permian Mass Extinction. *Science* **272**, 1155-1158 (1996).

[24] Berry, W. B. N. & Wilde, P. Progressive ventilation of the oceans; an explanation for the distribution of the lower Paleozoic black shales. *Am. J. Sci.* **278**, 257-275 (1978).

[25] Bambach, R. K., Knoll, A. H. & Wang, S. C. Origination, extinction, and mass depletions of marine diversity. *Paleobiology* **30**, 522-542 (2004).

[26] Palmer, A. R. Biomere: A New Kind of Biostratigraphic Unit. *Journal of Paleontology* **39**, 149-153 (1965).

[27] Scotese, C. R., *Atlas of Earth History* (Arlington, Texas, 2001).

[28] Ahlberg, P. *et al.* Cambrian high-resolution biostratigraphy and carbon isotope chemostratigraphy in Scania, Sweden: first record of the SPICE and DICE excursions in Scandinavia. *Lethaia*, 13 (2008).

[29] Lyons, T. W. & Severmann, S. A critical look at iron paleoredox proxies: New insights from modern euxinic marine basins. *Geochimica Cosmochimica Acta* **70**, 5698-5722 (2006).
[30] Raiswell, R., Buckley, F., Berner, R. A. & Anderson, T. F. Degree of pyritization of iron as a paleoenvironmental indicator of bottom-water oxygenation. *J. Sed. Res.* **58**, 812-819 (1988).

Author contributions BCG, TWL, MRS, SY collected samples used in this study. BCG did the chemical analyzes and collected mass spectrometer and ICP-MS data. BCG and LRK built the geochemical box model. BCG wrote the manuscript, with contributions from TWL, AHK and LRK. All the authors contributed to discussion and interpretations.

Acknowledgements NSF-EAR and NASA Astrobiology provided funding. Fieldwork and sample collection were aided by S. Bates, L. Bongers, H. Dayton, S. Mason, P. McGoldrick, J. Owens, C. Seeger, E. Starbuck. Sulphur isotope analyzes were aided by S. Bates and W. Gilhooly. Discussions with G. Love, N. Hughes, D. Johnston, P. Cohen and T. Dahl improved the manuscript.

Figure captions

Figure 1. Paleo-reconstruction of the later Cambrian Earth[27] showing locations where the SPICE has been identified (filled circles). Locations investigated in this study: Western Laurentia (WL) — Shingle Pass and Lawson Cove, Great Basin USA; Eastern Laurentia (EL) — TE-1 Texas County Core, Missouri, USA; Gondwana (GD) — Mount Whelan #1 and Mount Murray, Queensland, Australia; Baltica (BL) — Andrarum #3 core, Sweden.

Figure 2: Chemostratigraphies of the studied carbonate sections. Isotope data are plotted by stratigraphic height in meters. International series and stages are based on published biostratigraphy and most recent definitions of the subdivisions of the Cambrian (see Supplementary Material). Carbon isotopes profiles from Single Pass and Lawsons Cove

sections and Mt. Whelan #1 core are from references 8 and 10, respectively. The CAS sulphur isotope profile from Shingle Pass is from reference 15.

Figure 3: Chemostratigraphic data from the Alum Shale, Andrarum #3 Core, Sweden. Molybdenum, molybdenum/total organic carbon (Mo/TOC), total iron and aluminum and iron speciation data are plotted along side organic carbon and pyrite sulphur isotope data. Carbon isotope profile is from reference 28. Since Mo covaries with the concentration of organic matter in sediments[19], Mo concentrations have been normalized to TOC to correct for variations in organic content. Shaded regions of the degree of pyritization (DOP), Fe_{py}/Fe_{HR}, Fe_{HR}/Fe_T and Fe/Al plots display values that indicate anoxia and euxinia: Fe_T/Al values above 0.5 and Fe_{HR}/Fe_T above 0.4 indicate deposition under anoxic water columns[29], and DOP and Fe_{py}/Fe_{HR} values above 0.75 are conservatively diagnostic of euxinic environments[30]. Note that the decrease and minimum in Mo and Mo/TOC correspond to the initiation and peak of the carbon and sulfur isotope excursions, respectively.

Figure 4: Examples of the modeled carbon and sulfur isotope composition of the ocean during the SPICE. The sulfur isotope plot shows the effect of varying the magnitude of the transient increase in pyrite burial. In these simulations the burial of rates organic carbon and pyrite sulfur were increased for a half million years to create the isotope excursions. Organic carbon burial was doubled from $4.1*10^{18}$ to $8.2*10^{18}$ moles/Myrs and pyrite burial was increased from the steady state rate ($0.98*10^{18}$ moles/Myrs) by the

292 factors listed in the legend. Values in parenthesis are the molar carbon to sulfur (C/S)
293 ratios of the transient burial fluxes introduced into the model. The starting marine sulfate
294 concentration in these simulations was 1.5 mM.
295
296
297

298

Figure 1

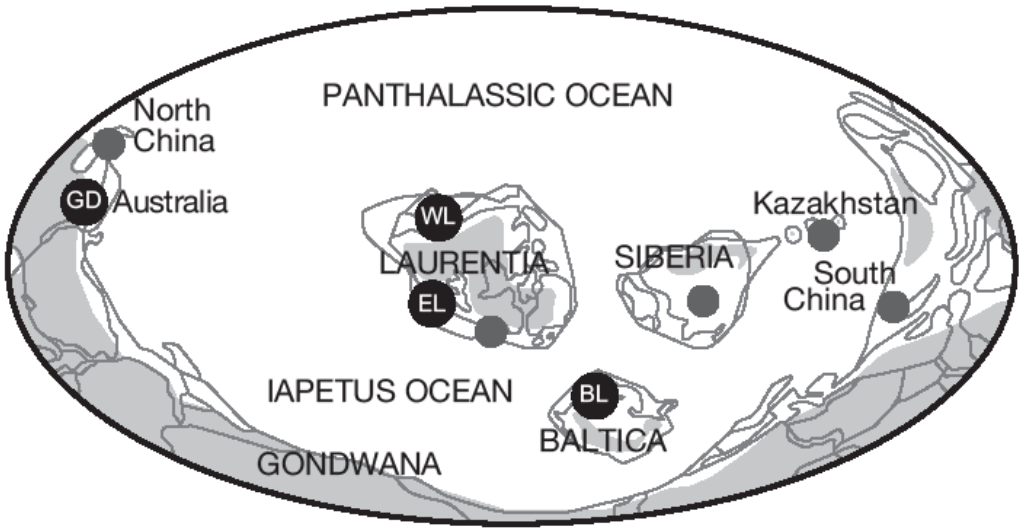

299

Figure 2

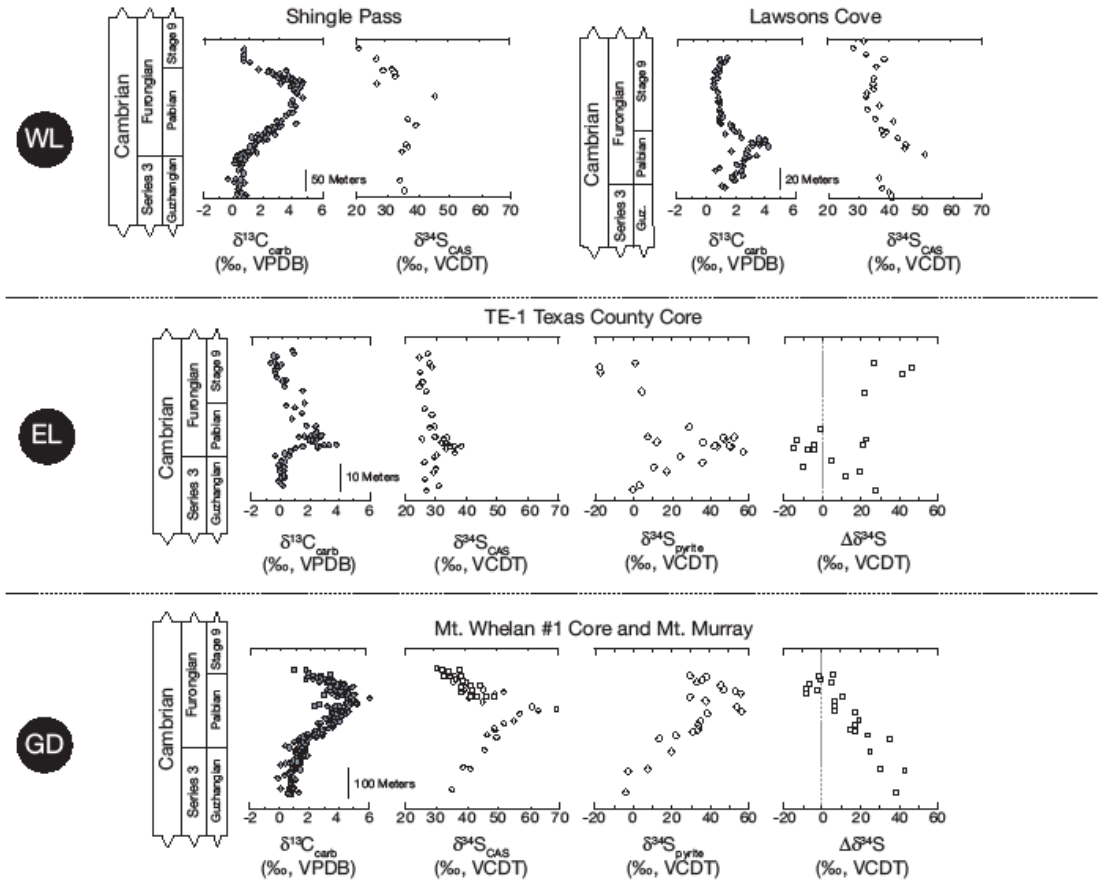

300
301

Figure 3

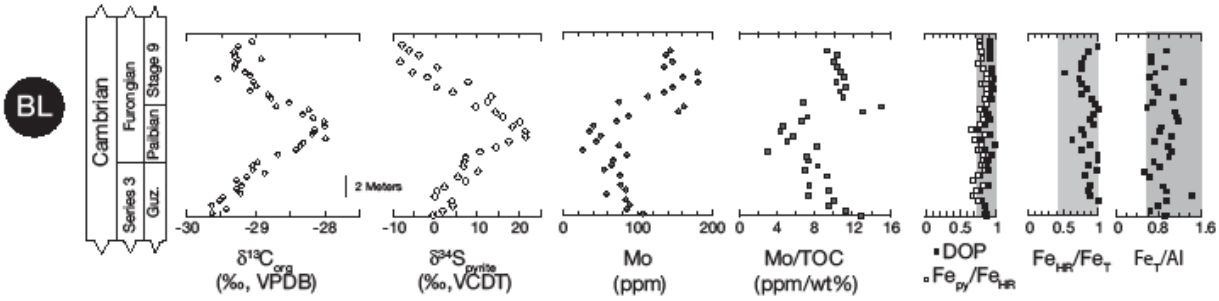
BL
Cambrian
Furongian
Stage 9
Paibian
Series 3
Guz.
2 Meters
-30
-29
-28
δ13Corg
(‰, VPDB)
-10
0
10
20
δ34Spyrite
(‰, VCDT)
0
100
200
Mo
(ppm)
0
4
8
12
16
Mo/TOC
(ppm/wt%)
0
0.5
1
DOP
Fepy/FeHR
0
0.5
1
FeHR/FeT
0
0.8
1.6
FeT/Al

302

Figure 4

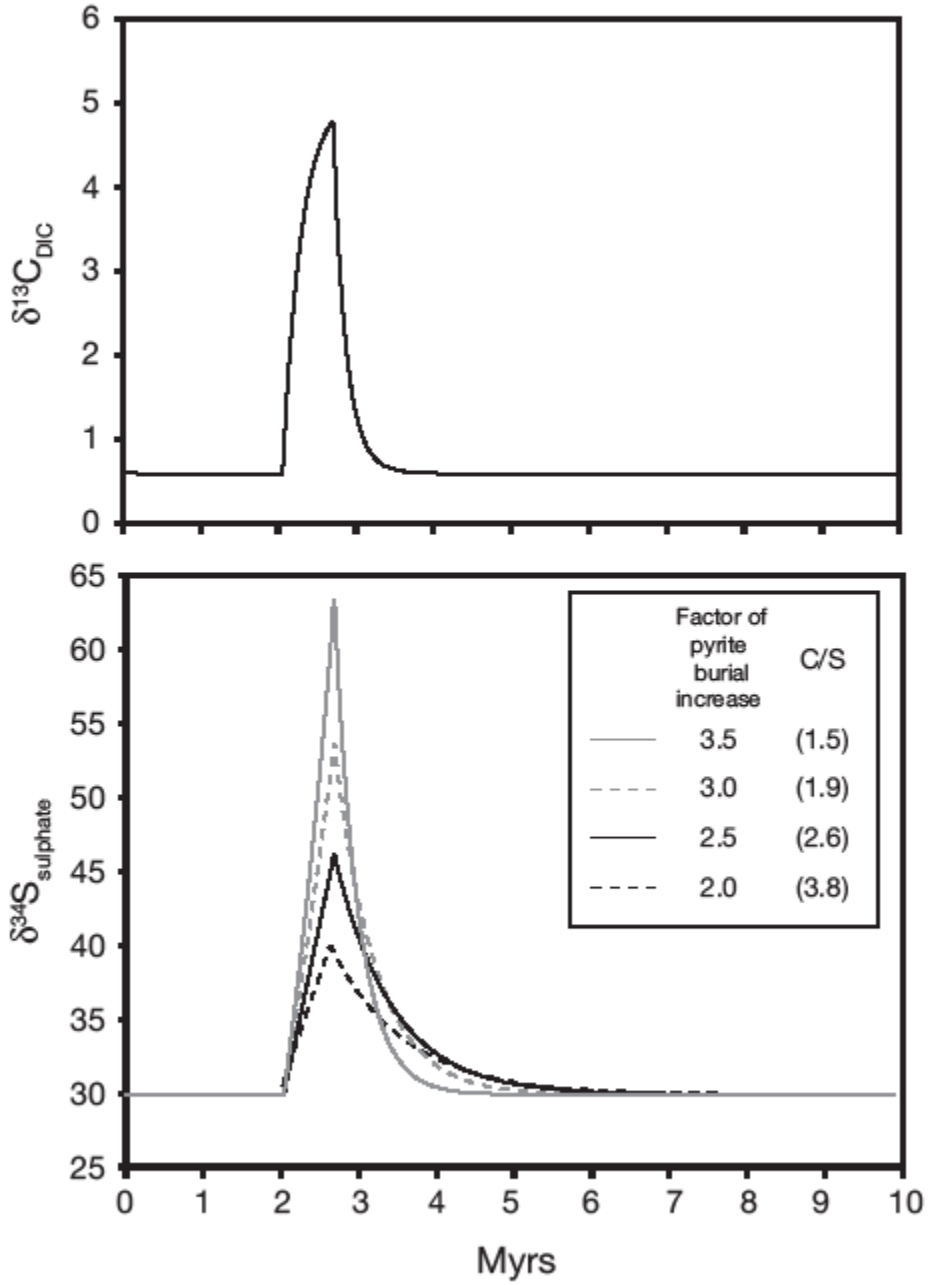

303
304